BIOCHEMISTRY
including biophysical chemistry & molecular biology

Rapid Report

pubs.acs.org/biochemistry

Long-Time Scale Fluctuations of Human Prion Protein Determined by Restrained MD Simulations

Massih Khorvash, Guillaume Lamour, and Jörg Gsponer*

Centre for High-Throughput Biology and Department of Biochemistry and Molecular Biology, University of British Columbia, East Mall, Vancouver, British Columbia V6T 1Z4, Canada

Supporting Information

ABSTRACT: Cellular prion protein (PrP^C) has the ability to trigger transmissible lethal diseases after in vivo maturation into a toxic amyloidogenic misfolded form (PrP^{Sc}). Here, we use hydrogen exchange protection factors in restrained molecular dynamics simulations to characterize long-time scale fluctuations in human PrP^C. We find that the regions of residues 138−141 and 183−192 form new β-strands in several exchange-competent structures. Moreover, these structural changes are associated with the disruption of native contacts that when tethered prevent fibril formation. Our findings illustrate the structural plasticity of PrP^C and are valuable for understanding the conversion of PrP^C to PrP^{Sc}.

Prion diseases are infectious and lethal neurodegenerative disorders that occur in humans as well as in animals.[1,2] Fundamental to these diseases is the conversion of an initially soluble, globular protein (PrP^C) into a misfolded, pathological form (PrP^{Sc}) that can aggregate and accumulate in the brain. Fourier transform infrared spectroscopy and circular dichroism showed that this conversion leads to a substantial change in the secondary structure of the prion protein.[3] While PrP^C has a high α-helical content (42%) and only a few residues in β-sheets (3%), PrP^{Sc} has a less pronounced α-helical content (30%) and is much richer in β-sheets (43%), which is consistent with its ability to form insoluble amyloid fibrils and its partial protease resistance. These findings suggest that the structural plasticity of PrP^C plays an important role in prion pathogenesis and emphasize the need for an improved understanding of the structure and dynamic behavior of this protein.

Here, we characterize the long-time scale fluctuations of human PrP^C by determining the structures of its exchange-competent state. The structures are calculated with the help of molecular dynamics (MD) simulations that use experimental hydrogen exchange (HX) protection factors as restraints. Such simulations make it possible to sample regions of the conformational space that correspond to rare fluctuations taking place on the millisecond time scale or longer time scales and, therefore, generate ensembles that contain those rare structures from which hydrogen exchange takes place. Specifically, the natural logarithm of the simulated protection factor of residue i is defined as $\ln P_i^{sim} = \beta_c N_i^c + \beta_h N_i^h$, where N_i^c and N_i^h are the number of native contacts and hydrogen bonds of residue i, respectively, and β_c and β_h previously fitted parameters.[4] During the restrained simulation, a pseudoenergy term penalizes deviations between experimental and simulated protection factors. Such simulations have previously been successfully used to characterize the exchange-competent states of Im7 and chymotrypsin inhibitor 2.[4,5]

We calculated the structural ensembles representing the exchange-competent state of human PrP^C(residues 125−228) by conducting 100 simulated annealing cycles with eight replicas and using 24 previously measured HX protection factors as restraints [for more details, see the Supporting Information (SI)].[6] The generated structures consistently reproduce the experimental HX protection factors (Figure 1A).

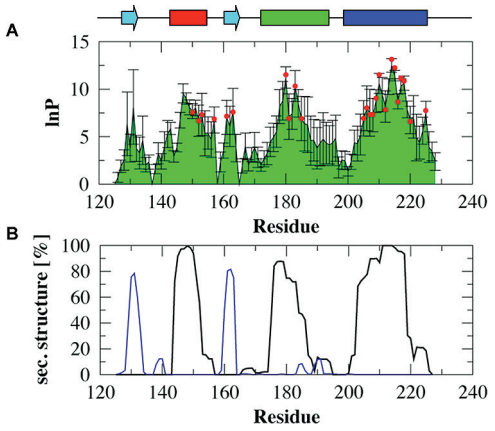

Figure 1. Prediction of HX protection factors and secondary structure content. (A) Comparison of ln P values of experimental protection factors[6] (red circles) with those back-calculated from the structures of the exchange-competent state (black line). The positions of the secondary structural elements (α-helices as boxes and β-strands as arrows) in the native state are indicated above the plot. (B) Averaged secondary structure content of the exchange-competent state with respect to the native state: α-helices (black) and β-strands (blue).

For a significant number of residues, no protection factors have been determined experimentally because of the lack of assignment or overly fast exchange. Most of these residues have an $\langle \ln P \rangle$ of $\leq$5. Significant exceptions are residues 143, 146−149, 177−179, 211, and 213. These residues have $\langle \ln P \rangle$ values of $\geq$5 because they are within the nearly fully folded helix I and

Received: August 11, 2011
Revised: October 20, 2011
Published: October 28, 2011

the folded parts of helices II and III (Figure 1B). Despite an experimental ln P of 7.5 for residue 225, the last turn of helix III is unfolded in most structures of the ensemble. No experimental protection factors could be measured for the C-terminal part of helix II. Consistently, all residues in segment 188−194 have a back-calculated $\langle \ln P \rangle$ of ≤ 5 and minimal helical structure in the exchange-competent state. Several nuclear magnetic resonance (NMR) studies of wild-type or mutant hamster and mouse PrP^C have recently shown that the C-terminal half of helix II is partially disordered and highly dynamic on the pico- to nanosecond time scale at pH ≤ 5.5.[7,8]

Our calculations show that the last three turns of helix II (residues 182−194), which are lost in most exchange-competent structures, are partially replaced by β-strands (residues 183−192) in ~10% of the structures (Figure 1B). In addition, residues 138−141 are involved in new β-sheet interactions in some structures of the exchange-competent state. Interestingly, recent NMR investigation of the urea-denatured state of human PrP^C identified three areas with strong β-strand structural preferences: residues 135−142, 157−165, and 182−189.[9] While the region of residues 157−165 harbors the second β-strand of the native state, the segments of residues 135−142 and 182−189 are not involved in any β-sheet interaction in the native state. Our simulations reveal that the latter two sequence segments, residues 135−142 and 182−189, form β-strands in at least 10% of the structures of the exchange-competent state.

To confirm that this finding is not purely incidental, we conducted three control simulations. We calculated new structural ensembles by using the same simulation protocol as before but leaving out one experimentally measured protection factor in each simulation. Then we checked whether the new ensembles (i) allowed prediction of the omitted protection factor and (ii) contained structures with β-strands in the segments of residues 138−141 and 183−192. In all control calculations, the omitted experimental protection factor is within one standard deviation of the back-calculated one (SI Figure 1). More importantly, new β-strands are found in the segments of residues 138−141 and 183−192 in all controls.

Next, we performed a cluster analysis to identify the most relevant conformational substates. The six largest clusters comprise more than 60% of the conformations in the calculated ensemble of the exchange-competent state (Figure 2) and represent the most relevant substates as shown by a principal component analysis (SI Figure 2a). In the first four clusters (Figure 2B−E), the native topology is conserved to a large extent and root-mean-square deviations of the Cα atoms (Cα-rmsds) from the native state vary between 6 and 10 Å. Nevertheless, changes are found at the level of the secondary structure. Helix II has lost three C-terminal turns in clusters 1, 3, and 4, and the native β-sheet is absent in cluster 2. Only minor structural changes are found for native helices I and III in the first four clusters. More substantial structural changes are found in clusters 5 and 6 (Figure 2F,G). Structures in both clusters have Cα-rmsds from the native state of 11 Å and lost the native topology. Besides a nearly fully unfolded helix II, helices I and III lack the first N-terminal turn. In addition, new β-strands are found in both clusters 5 and 6. In cluster 5, the native, antiparallel β-sheet has an additional strand formed by residues 185−187. By contrast, a new parallel β-sheet is present in the structures of cluster 6. This new β-sheet is formed by residues 138−141 and 189−192.

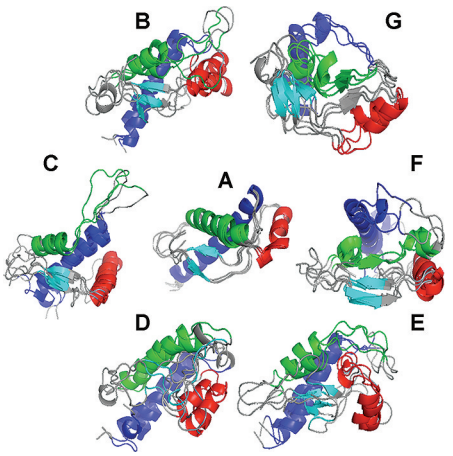

Figure 2. Exchange-competent state of human PrP^C. (A) NMR structure of the native state of human PrP^C (residues 125−228).[11] (B−G) Representative structures of the six largest clusters of the exchange-competent state. Segments that contain native α-helices I−III are colored red, green, and blue, respectively. Native β-strands are colored cyan.

Recently, Hafner-Bratkovic et al.[10] engineered new disulfide bridges into mouse PrP^C to map the regions that require major structural rearrangements for the fibrillization process. It was shown that only disulfide bridges that tether subdomain 1, containing helix I and the native β-sheet, with subdomain 2, containing helices II and III, prevent PrP conversion and fibrillization (SI Figure 3).

For the six largest clusters of the exchange-competent state, we calculated the average spatial separation between amino acid pairs that have been mutated to cysteines by Hafner-Bratkovic[10] to introduce the new disulfide bridges (Table 1). Most mutated pairs have a spatial separation that is very close to the one measured for the native state, i.e., a separation that is compatible with a disulfide bridge. However, the mutated pairs (134/217, 137/212, and 161/213) are more than 10 Å farther apart in clusters 5 and 6 than in the native state. Interestingly, these are exactly the pairs that when connected by a disulfide bridge prevent conversion of mouse PrP^C in vitro.[10] In additional control calculations, in which we used the same protocol as before but tethered residue pairs 134/217 and 161/213 by a restraint, the β-sheet-enriched conformational substates of clusters 5 and 6 were not sampled any more (SI Figure 2b and SI text). These controls suggest that the formation of new β-strands in the exchange-competent state is facilitated by disruption of the same native contacts that when tethered prevented fibrillization in vitro. This is an interesting finding that could suggest that the large conformational changes observed in some structures of the exchange-competent state may initiate or participate in the conversion of PrP^C. It is important to note that the structural changes leading to large spatial separation of residue pairs 134/217, 137/212, and 161/213 are not associated with a significant increase in the radius of gyration of PrP^C and a clear separation of subdomains 1 and 2. All clusters have radii of gyration that vary between 14.0 and 15.4 Å, compared to 14.1 Å for the native state. Hafner-Bratkovic et al.[10] proposed that a separation of subdomains 1 and 2 is necessary for conversion of PrP^C. Further experimental and theoretical studies are necessary to clarify this question.

dx.doi.org/10.1021/bi2012756|*Biochemistry* 2011, 50, 10192−10194

Table 1. Average Spatial Separation (angstroms) between Residue Pairs in the Native and Exchange-Competent State[a]

	128/162	134/217[b]	136/154	137/212[b]	141/146	161/183	161/213[b]	176/211	191/196
native	6.6 ± 0.3	9.1 ± 0.4	7.0 ± 0.4	6.8 ± 0.2	6.5 ± 0.2	5.9 ± 0.1	6.9 ± 0.1	6.3 ± 0.2	5.9 ± 0.2
cluster 1	6.9 ± 1.9	7.8 ± 1.5	10.0 ± 2.3	8.8 ± 2.0	6.9 ± 1.3	5.7 ± 0.8	7.9 ± 1.3	6.0 ± 0.6	9.8 ± 2.1
cluster 2	6.9 ± 1.6	8.2 ± 1.6	9.0 ± 1.6	10.5 ± 2.0	6.6 ± 1.0	5.8 ± 0.6	7.8 ± 0.6	6.1 ± 0.4	8.2 ± 1.8
cluster 3	11.9 ± 3.1	**23.9 ± 2.0**	12.1 ± 1.2	**16.9 ± 1.8**	5.7 ± 0.4	6.3 ± 0.8	7.6 ± 1.3	5.9 ± 0.4	11.2 ± 3.0
cluster 4	8.9 ± 1.5	7.7 ± 1.0	13.0 ± 1.0	10.7 ± 1.8	6.5 ± 0.4	5.8 ± 0.6	7.7 ± 1.0	5.7 ± 0.5	11.6 ± 1.7
cluster 5	5.9 ± 0.5	**18.1 ± 2.1**	10.5 ± 1.2	**17.0 ± 1.7**	6.1 ± 0.4	9.5 ± 1.3	**18.1 ± 1.3**	6.1 ± 0.4	5.6 ± 0.4
cluster 6	5.3 ± 0.3	**23.6 ± 5.2**	8.3 ± 1.0	**25.8 ± 2.4**	8.9 ± 0.5	14.7 ± 4.5	**28.7 ± 4.5**	6.6 ± 0.6	10.6 ± 0.6

[a]Residue pairs that are more than 10 Å farther apart in the structures of a cluster than in the native state are shown in bold. [b]Residue pairs that prevent conversion when tethered.

In summary, we characterized the exchange-competent state of human PrP^C with the help of MD simulations that use experimental HX protection factors as restraints. The simulations revealed substantial structural changes in large parts of PrP^C in this state. Specifically, the C-terminal part of helix II is largely unfolded or in a new β-strand conformation. These findings are consistent with several recent NMR and simulation studies that document substantial dynamics for the second part of helix II on different time scales and under various pH conditions.[7,8,12,13]

An important finding of our calculations is that the unfolding of the C-terminus of helix II leads to the formation of new β-strands in some structures of the exchange-competent state. The new strands form in regions that have been shown to have β-strand structural preferences in the urea-denatured state of human PrP.[9] In addition, our results are consistent with recent experiments and simulations that indicate that helices II and III are crucial to the conversion of PrP^C to PrP^{Sc} and are part of the amyloid fibril core.[14−16] Interestingly, MD simulations by Chakroun et al. showed that helices II and III can form a stable β-sheet structure that is nucleated by the segments of residues 183 and 184 and residues 215 and 216.[17] These and our findings support the hypothesis that the C-terminal part of helix II may participate in the conversion of PrP^C. Further support for this hypothesis comes from our observation that the structural changes leading to increased β-sheet content are associated with disruption of contacts that when tethered prevent fibrillization of PrP^C. It is important to note that it is likely that other regions are also involved in the conversion process. Moreover, it is not clear whether conversion and fibril formation could start from structures that are part of the exchange-competent state or whether further or complete unfolding is required. Nevertheless, our study provides valuable insights into the dynamics of PrP^C and contributes to an improved understanding of the conversion mechanisms of this protein.

■ ASSOCIATED CONTENT

Supporting Information

Figures 1−4, detailed methods, and discussion. This material is available free of charge via the Internet at http://pubs.acs.org.

■ AUTHOR INFORMATION

Corresponding Author

*E-mail: gsponer@chibi.ubc.ca. Phone: (604) 827-4731. Fax: (604) 822-2114.

Funding

Supported by a PrioNet Canada Recruitment Grant.

■ REFERENCES

(1) Prusiner, S. B., Scott, M. R., DeArmond, S. J., and Cohen, F. E. (1998) *Cell 93*, 337−348.
(2) Aguzzi, A., Heikenwalder, M., and Polymenidou, M. (2007) *Nat. Rev. Mol. Cell Biol. 8*, 552−561.
(3) Pan, K. M., Baldwin, M., Nguyen, J., Gasset, M., Serban, A., Groth, D., Mehlhorn, I., Huang, Z., Fletterick, R. J., Cohen, F. E., et al. (1993) *Proc. Natl. Acad. Sci. U.S.A. 90*, 10962−10966.
(4) Best, R. B., and Vendruscolo, M. (2006) *Structure 14*, 97−106.
(5) Gsponer, J., Hopearuoho, H., Whittaker, S. B., Spence, G. R., Moore, G. R., Paci, E., Radford, S. E., and Vendruscolo, M. (2006) *Proc. Natl. Acad. Sci. U.S.A. 103*, 99−104.
(6) Hosszu, L. L., Baxter, N. J., Jackson, G. S., Power, A., Clarke, A. R., Waltho, J. P., Craven, C. J., and Collinge, J. (1999) *Nat. Struct. Biol. 6*, 740−743.
(7) Bae, S.-H., Legname, G., Serban, A., Prusiner, S. B., Wright, P. E., and Dyson, H. J. (2009) *Biochemistry 48*, 8120−8128.
(8) Bjorndahl, T. C., Zhou, G. P., Liu, X., Perez-Pineiro, R., Semenchenko, V., Saleem, F., Acharya, S., Bujold, A., Sobsey, C. A., and Wishart, D. S. (2011) *Biochemistry 50*, 1162−1173.
(9) Gerum, C., Silvers, R., Wirmer-Bartoschek, J., and Schwalbe, H. (2009) *Angew. Chem., Int. Ed. 48*, 9452−9456.
(10) Hafner-Bratkovic, I., Bester, R., Pristovsek, P., Gaedtke, L., Veranic, P., Gaspersic, J., Mancek-Keber, M., Avbelj, M., Polymenidou, M., Julius, C., Aguzzi, A., Vorberg, I., and Jerala, R. (2011) *J. Biol. Chem. 286*, 12149−12156.
(11) Zahn, R., Liu, A., Luhrs, T., Riek, R., von Schroetter, C., Lopez Garcia, F., Billeter, M., Calzolai, L., Wider, G., and Wuthrich, K. (2000) *Proc. Natl. Acad. Sci. U.S.A. 97*, 145−150.
(12) Chebaro, Y., and Derreumaux, P. (2009) *J. Phys. Chem. B 113*, 6942−6948.
(13) Rossetti, G., Giachin, G., Legname, G., and Carloni, P. (2010) *Proteins 78*, 3270−3280.
(14) Lu, X., Wintrode, P. L., and Surewicz, W. K. (2007) *Proc. Natl. Acad. Sci. U.S.A. 104*, 1510−1515.
(15) Adrover, M., Pauwels, K., Prigent, S., de Chiara, C., Xu, Z., Chapuis, C., Pastore, A., and Rezaei, H. (2010) *J. Biol. Chem. 285*, 21004−21012.
(16) Dima, R. I., and Thirumalai, D. (2002) *Biophys. J. 83*, 1268−1280.
(17) Chakroun, N., Prigent, S., Dreiss, C. A., Noinville, S., Chapuis, C., Fraternali, F., and Rezaei, H. (2010) *FASEB J. 24*, 3222−3231.